Ceramics International xxx (xxxx) xxx–xxx

Contents lists available at ScienceDirect

Ceramics International

journal homepage: www.elsevier.com/locate/ceramint

Grain-orientation-engineered textured $BaMoO_4$: Eu^{3+} luminescent thin film

Fengjun Chun, Wen Deng, Binbin Zhang, Wen Li, Meilin Xie, Chao Luo, Weiqing Yang*

Key Laboratory of Advanced Technologies of Materials (Ministry of Education), School of Materials Science and Engineering, State Key Laboratory of Traction Power, Southwest Jiaotong University, Chengdu, 610031, China

ARTICLE INFO

Keywords:
Orientation engineering
Textured thin films
PAD
$BaMoO_4$: Eu^{3+}
Photoluminescence

ABSTRACT

Rare-earth-doped luminescent thin films have been responsible for unprecedented positive impacts in optoelectronic devices with high lateral resolution, excellent thermal stability, and strong adhesion to the solid surface. However, limited emission intensity and high-cost fabrication routine deeply inhibit their practical and commercial applications. Here, we propose a grain orientation engineering strategy via simple and low-cost polymer-assisted deposition (PAD) to fabricate textured $BaMoO_4$: Eu^{3+} thin films with highly improved emission intensity by reducing the lattice mismatch between the thin films and substrates. The high-quality < 004 > -textured $BaMoO_4$: Eu^{3+} thin film mounted on the (001)-oriented Si substrate with the Lotgering factor F_{004} of 94.6%, boosting up the emission intensity of which to 366% compared to their randomly oriented counterparts. Moreover, the as-fabricated $BaMoO_4$: Eu^{3+} film shows strong red emission at 615 nm corresponding to the $^5D_0 \rightarrow {}^7F_2$ transition of Eu^{3+} with correlated color temperature (CCT) of 2922 °C and ultra-high color purity (nearly 100%). Furthermore, the geometry, size, and luminescence performance of the crystals can be precisely manipulated by tuning the growth temperature, layers of the film, and doping concentration. The present research offers a novel and low-cost route to engineer luminescent films with controllable orientation and enhanced emission intensity, which demonstrate great potentials towards practical applications and industrialization.

1. Introduction

Compared with phosphors crystals and powders, the rare-earth-doped luminescent thin films possess merits of higher contrast and resolution, superior thermal conductivity, greater uniformity as well as better adhesion to the solid substrate, attracting great interest in optoelectronic devices, ranging from bio imaging, drug delivery, solid state lasers, flat panel displays, integrated optics systems and many others [1–6]. Among these, the rare-earth elements doped scheelite tetragonal structured molybdate thin films have been increasingly important since the compelling of outstanding physicochemical stability and excellent photoelectric properties [7–11]. Especially, europium (Eu) doped $BaMoO_4$ various luminescent materials have received considerable attention due to its characteristic red emission of Eu^{3+} at around 615 nm with potential applications in warm white light-emitting diodes (LEDs), lasers, display devices, to name a few [12–16].

Nevertheless, the current approaches to fabricate the luminescent films including pulsed laser deposition, sputtering, molecular beam epitaxy, chemical vapor deposition and spray pyrolysis generally suffer from the low luminescence efficiency, complicated manufacturing process and inaccurate regulation for the concentration of the rare-earth ions, which largely overshadows their further adoption in industrial-scale [17–19]. It is urgently needed to develop a feasible, low-cost, and controllable method to prepare high-performance luminescent thin films. In our previously reported works, the PAD method has been proved as a simple and low-cost pathway to generate luminescent thin films on the various substrates which can precisely regular the concentration of doping ions [6,8]. However, the emission intensity of the luminescent thin films fabricated by PAD is relatively low for practical application owing to their large lattice mismatch with the substrate, indicating that the interface controllability is still a big challenge.

Herein, we propose a grain orientation engineering strategy to remedy the defects caused by lattice mismatch, meanwhile, highly orientated $BaMoO_4$: Eu^{3+} thin films are fabricated with significant enhancement of the luminescence properties. The monocrystal silicon (Si) is picked as substrates owing to its low cost and superior lattice compatibility, on which the $BaMoO_4$: Eu^{3+} thin films are mounted [20–22]. To justify three effect of the orientation on the luminescence performance, three different oriented Si substrates are exploited to mount $BaMoO_4$: Eu^{3+} thin films. The $BaMoO_4$: Eu^{3+} thin films mounted on (111)-oriented Si substrates exhibit randomly orientation, while the $BaMoO_4$: Eu^{3+} thin films mounted on (100)-oriented and (001)-

* Corresponding author.
E-mail address: wqyang@swjtu.edu.cn (W. Yang).

https://doi.org/10.1016/j.ceramint.2020.07.208
Received 11 July 2020; Received in revised form 20 July 2020; Accepted 21 July 2020

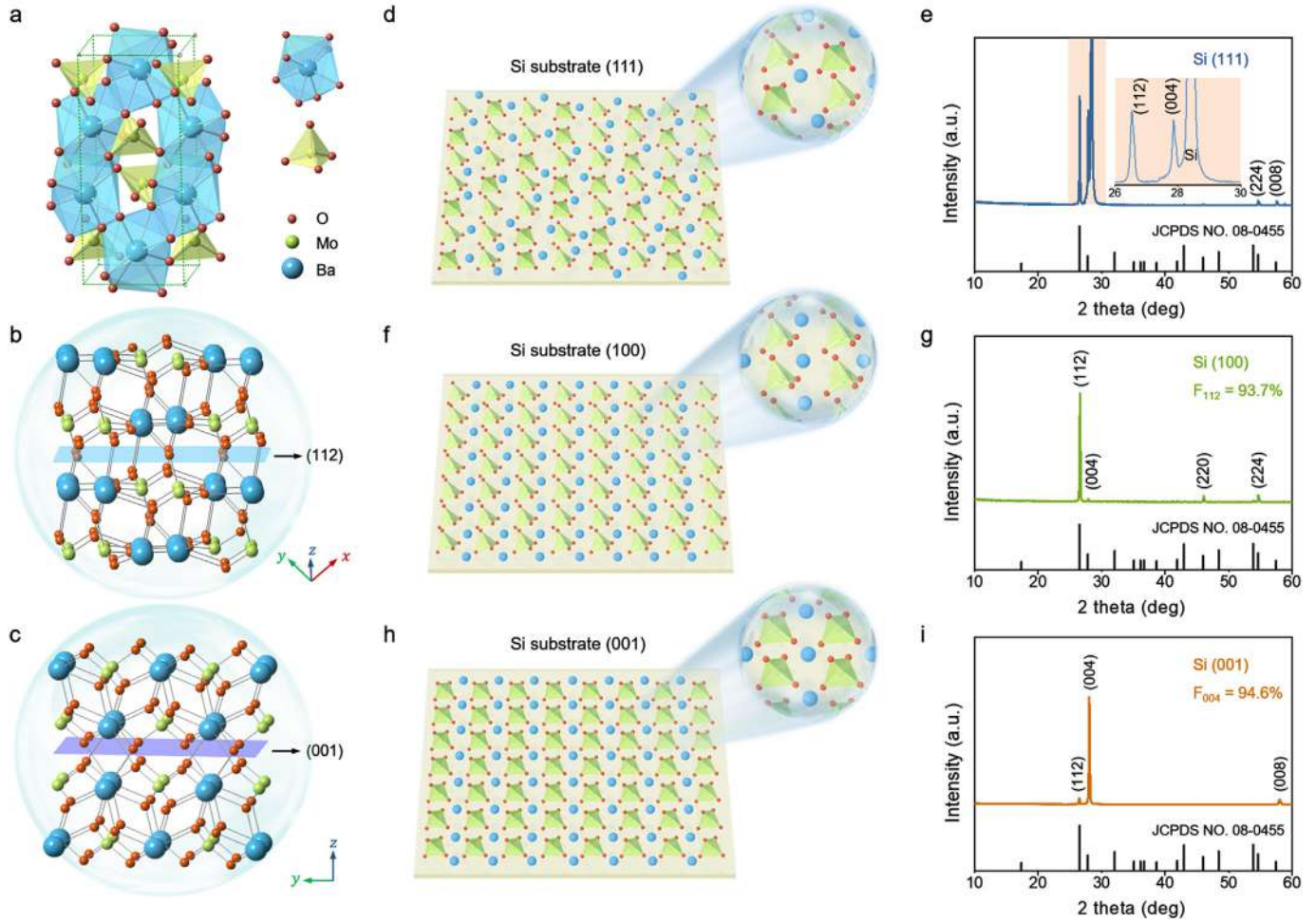

Fig. 1. The crystal structure of $BaMoO_4$: Eu^{3+} thin films. (a) Unit cell representation of $BaMoO_4$. (b) Schematic representations of (112) surface. (c) Schematic representations of (001) surface. (d) Schematic of the crystal structure of nontextured $BaMoO_4$: Eu^{3+} thin film. (e) XRD pattern of nontextured $BaMoO_4$: Eu^{3+} structure. (f) Schematic of the crystal structure of < 112 > -textured $BaMoO_4$: Eu^{3+} thin film. (g) XRD pattern of < 112 > -textured $BaMoO_4$: Eu^{3+} thin film. (h) Schematic of the crystal structure of < 004 > -textured $BaMoO_4$: Eu^{3+} thin film. (i) XRD pattern of < 004 > -textured $BaMoO_4$: Eu^{3+} thin film.

oriented Si substrates exhibit < 112 > -preferred and < 004 > -preferred orientation, respectively. The luminescence intensity of high-quality < 004 > -textured $BaMoO_4$: Eu^{3+} thin films can be improved 366% compared with the nontextured one. Furthermore, the luminescence performance of $BaMoO_4$: Eu^{3+} thin films can be further enhanced via tuning the annealing temperature, layers of thin film and concentration of Eu^{3+} ions. The $BaMoO_4$: Eu^{3+} thin films exhibit bright red emission at 615 nm corresponding to the $^5D_0 \rightarrow {}^7F_2$ transition of dopant Eu^{3+} ions, uniform morphology, ultra-high color purity of nearly 100%, and correlated color temperature (CCT) of 2922 ˚C. Therefore, this demonstrated grain orientation engineering could open a door for the low-cost and high luminescence intensity thin films, which accelerates the progress of practical applications and industrialization.

2. Experimental section

2.1. Preparation of precursor solution

EDTA (99.99%, Aldrich), PEI (99.99%, Aladdin), $Ba(NO_3)_2$ (AR, Keshi), $(NH_4)_6Mo_7O_{24}{\cdot}4H_2O$ (AR, Keshi), and $EuCl_3{\cdot}6H_2O$ (99.99%, Aladdin) were used as the starting materials, and all the starting materials were used without further purification. 1g EDTA and 1g PEI were completely dissolved in 40 mL deionized water, then 1g $Ba(NO_3)_2$ were added slowly and stirred well to form a homogeneous solution. The solution was transferred into an Amicon filtration of 50 ml capacity, and it was filtrated at least 3 times under the pressure of N_2. The actual concentration of Ba^{2+} ions in the precursor solution was confirmed by inductively coupled plasma atomic emission spectroscopy (ICP-AES) and the concentration is 20.22 mg/mL. Similarly, the solution of Mo^{6+} and Eu^{3+} was obtained by the above experiment approach and the actual concentration of Mo^{6+} and Eu^{3+} is 15.58 mg/mL and 13.52 mg/mL, respectively. Finally, the solution of Ba^{2+}, Mo^{6+} and Eu^{3+} were mixed at the desired molar ration of 1: 1: x (x = 0.01-0.06) to obtain the precursor solution of $BaMoO_4$: Eu_x^{3+}.

2.2. The growth of $BaMoO_4$: Eu^{3+} thin films on different oriented Si substrates

The $BaMoO_4$: Eu^{3+} thin films were mounted on monocrystalline Si substrates with different orientations by the PAD method, the substrates including (111)-oriented, (100)-oriented and (001)-oriented Si. Prior to deposition, comprehensive cleaning of substrates was carried out by using acetone, ethanol, and deionized water. The precursor solution of $BaMoO_4$: Eu_x^{3+} was spin-coated on clean substrates at 1000 rpm for 10 s and 3000 rpm for 20 s, then baked on a heating stage at 100 ˚C to remove the residual water. After that, these samples were thermally treated according to the self-designed procedure in a muffle furnace as design. The processes of spin coating and thermal treatment were repeated several times depending on the need for thin-film thickness.

2.3. Characterization

The crystal structure and orientation of $BaMoO_4$: Eu^{3+} thin films were analyzed by the X'Pert Pro (Holland) X-ray diffract meter with Cu K_{a1} radiation (λ = 0.15406 nm) for 2θ values in the range of 10–60°. The morphology and grain size distribution of $BaMoO_4$: Eu^{3+} thin films were identified by the FEI QUANTA FEG 250 scanning electron microscopy (SEM, S4800). The PL emission and excitation spectra of samples were measured using the FLS980 (Edinburgh Instruments) spectrometer with a 450 W Xenon lamp. The decay curves were recorded by the FLS980 spectrometer with a 60 W μs pulsed Xenon flash lamp at room temperature.

3. Result and discussion

The three-dimensional unit cell structure schematic representations of $BaMoO_4$ is presented in Fig. 1a, the structure was modeled according to the ICSD #50821. The structural of $BaMoO_4$ belong to the scheelite structure (tetragonal. $I4_1/a$ (No. 88)), and the lattice parameters are $a = b = 5.5479$ Å, $c = 12.745$ Å, $V = 392.22$ Å and $Z = 4$ [15,16]. The Ba atoms are bonded to eight oxygens to form the polyhedral [BaO_8] clusters, and Mo atoms are coordinated to four oxygens to form the tetrahedral [MoO_4] clusters [23]. In the unit cell (Z = 4) of $BaMoO_4$, Ba atoms occupy the 4b sites, Mo atoms occupy the 4a sites, and O atoms occupy the 16f sites. The crystal structures of surfaces (112) and (001) are presented in Fig. 1b and c. Due to the ionic radius of Eu^{3+} (1.07 Å) is smaller than the Ba^{2+} (1.42 Å) ionic radius, Eu^{3+} ions are more likely to occupy the site of Ba^{2+} ions [16]. The XRD patterns of $BaMoO_4$: $Eu^{3+}_{0.05}$ thin films mounted on the different substrate are illustrated in Fig. 1e, g and 1i. The diffraction peaks of these three samples are in good agreement with XRD reference data (JCPDS No. 08-0455) of $BaMoO_4$, there are no additional peaks were found [24]. The phase purity of samples indicates that Eu^{3+} ions were successfully incorporated into the $BaMoO_4$ host lattice as activators. The grain orientation of $BaMoO_4$: Eu^{3+} thin films can be controlled by using various-oriented Si substrates. Schematic of the crystal structure of nontextured and textured $BaMoO_4$: Eu^{3+} thin films were illustrated in Fig. 1d, f and 1h. The nontextured $BaMoO_4$: Eu^{3+} thin film mounted on the (111)-orientated Si substrate shows two major orientations of (112) and (004), as shown in Fig. 1d and e. The high-quality textured samples can be fabricated using Si substrate with (100) orientation and (001) orientation. As shown in Fig. 1f and g, the < 112 > -textured sample shows an obvious enhancement in the intensity of (112) diffraction peaks, the Lotgering factor F_{112} of the sample is 93.7% [25]. The < 004 > -textured sample shows a significant enhancement in the intensity of (004) diffraction peak, and the sample's Lotgering factor F_{004} is as high as 94.6%, as illustrated in Fig. 1h and i. The ultra-high Lotgering factor reveals the strong (004)-preferred orientation of the $BaMoO_4$: Eu^{3+} thin films [26]. Marisa et al. suggested that the surface energies of the (001) and (112) orientation are lowest in the $BaMoO_4$ crystal, it indicates that the (004) and (112) texture of the luminescent thin films easier to form [27]. The lower surface energy of (004) will drive the $BaMoO_4$: Eu^{3+} thin films mounted on (001)-oriented Si substrate with higher orientation.

In order to investigate the effect of texture on luminescence properties, the excitation and emission spectra of nontextured, < 112 > -textured and < 004 > -textured $BaMoO_4$: Eu^{3+} thin films have been recorded, as illustrated in Fig. 2. It is clearly seen that the excitation spectra of $BaMoO_4$: Eu^{3+} thin films possess a broadband excitation from 280 to 320 nm, which is assigned to the charge transfer of $O^{2-} \rightarrow Mo^{6+}$ in the [MoO_4^{2-}] group and $O^{2-} \rightarrow Eu^{3+}$ [28]. The excitation peaks at 392, 424, 440nm and 493 nm corresponding to the transitions of $^7F_0 \rightarrow {}^5L_6$, $^7F_0 \rightarrow {}^5D_3$, $^7F_0 \rightarrow {}^5D_2$, and $^7F_0 \rightarrow {}^5D_1$, respectively, as shown in Fig. 2a. The emission spectra can be attributed to $^5D_1 \rightarrow {}^7F_1$, $^5D_0 \rightarrow {}^7F_1$, $^5D_0 \rightarrow {}^7F_2$, $^5D_0 \rightarrow {}^7F_3$, $^5D_0 \rightarrow {}^7F_4$ transitions, and these spectra peaked at 532, 590, 615, 652, 700 nm, respectively, as shown in Fig. 2b [29]. The narrow peaks at 615 nm have high emission intensity and contribute a lot to the red emission. Compared with nontextured thin films, the < 112 > -oriented and < 004 > -oriented $BaMoO_4$: Eu^{3+} thin films show higher luminescence intensities. The emission intensity of < 004 > -oriented $BaMoO_4$: Eu^{3+} thin film is enhanced to 366% compared with the nontextured thin film. This enhanced luminescence intensity of the textured film can be attributed to less lattice mismatch between $BaMoO_4$: Eu^{3+} thin film and Si substrate.

Fig. 3 shows the SEM images of $BaMoO_4$: Eu^{3+} thin films, it can be seen the morphology is distinguishing of the < 004 > -textured and < 112 > -textured $BaMoO_4$: Eu^{3+} thin films. As illustrated in Fig. 3a, b and 3c, the < 004 > -textured $BaMoO_4$: Eu^{3+} thin films are composed of smooth spherical particles with uniform size, and the average particle size is 0.53 μm. The $BaMoO_4$: Eu^{3+} grains are independent and not in contact because the thin film grow perpendicular to the substrate [30,31]. And the smooth surface of the particles also indicates a less lattice mismatch between $BaMoO_4$: Eu^{3+} thin film and (001)-oriented substrate. As shown in Fig. 3d, e and 3f, the particles of < 112 > -textured $BaMoO_4$: Eu^{3+} thin film are irregularities and they were partly physically overlapped. The average size of these particles is 0.72 μm, these larger and flatter particles are due to the interaction between the thin film and the (100)-oriented substrate.

Based on the above comparison analysis, the (001)-oriented Si substrate was exploited as the fixed substrate for mounting a series of $BaMoO_4$: Eu^{3+} thin films. It is well known that the crystallinity of the thin film is closely associated with the emission intensity, and optimizing the annealing temperature is the most effective way to increase the crystallinity of $BaMoO_4$: Eu^{3+} thin films. The temperature-dependent emission spectra of $BaMoO_4$: Eu^{3+} thin films are illustrated in Fig. 4a. The emission intensity reaches its maximum value when the annealing treatment temperature is 700 °C (Fig. 4b), this is consistent with the XRD results. As shown in Fig. 4c, the $BaMoO_4$: Eu^{3+} thin film annealed at 700 °C shows the best crystallinity and texture quality. In this work, we use a multi-layer film structure to overcome the shortcomings of uncontrollable film thickness and low luminescent efficiency. Fig. 4d and e shows the emission spectra and intensity of $BaMoO_4$: Eu^{3+} thin films with different layers, the position of the emission peaks is fixed while the intensity is increased gradually. The increased layers are conducive to increasing the emitting volume, resulting in increased emission intensity. As the number of layers increases, the rate of increase in emission intensity gradually slows and reaches saturation. The doping concentration of Eu^{3+} is also strongly related to the luminescence performance of $BaMoO_4$: Eu^{3+} thin films. As shown in Fig. 4f and g, the emission intensity of $BaMoO_4$: Eu^{3+} thin films increase first and then decreases, and the optimal doping concentration of Eu^{3+} is 5%. Although the increase in doping concentration will increase in the emission center, a higher doping concentration will result in a closer distance between dopants, which will accelerate the energy transfer between adjacent Eu^{3+}. The concentration quenching inevitably occurs when the doping concentration continues to increase.

In order to better understand the excitation and emission process of Eu^{3+} in $BaMoO_4$, an energy level diagram is illustrated in Fig. 5a. The luminescence decay curves were employed to understand the information of the energy migration among Eu^{3+} ions. The decay curves of $BaMoO_4$: Eu^{3+} thin films are presented in Fig. 5b. All the samples are well fitted with the biexponential equation below [32,33]:

$$I(t) = A_1 e^{-t/\tau_1} + A_2 e^{-t/\tau_2} \quad (1)$$

Where *I(t)* is the emission intensity corresponding to the time *t*, A_1 and A_2 refer to the constant; τ_1 and τ_2 are fast and slow fluorescent lifetimes. Further, the average decay time (τ*) can be calculated by the equation as follows:

$$\tau^* = (A_1\tau_1^2 + A_2\tau_2^2)/(A_1\tau_1 + A_2\tau_2) \quad (2)$$

All the values are summarized in Table 1. The calculated τ* of the

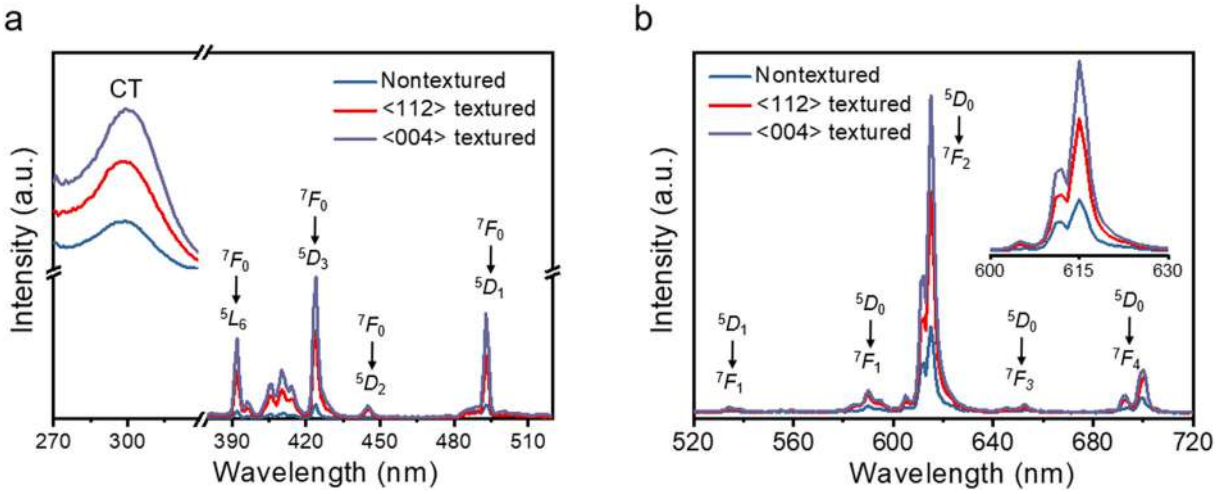

Fig. 2. The excitation (a) and emission (b) spectra of nontextured, < 112 > -textured and < 004 > -textured $BaMoO_4$: Eu^{3+} thin films.

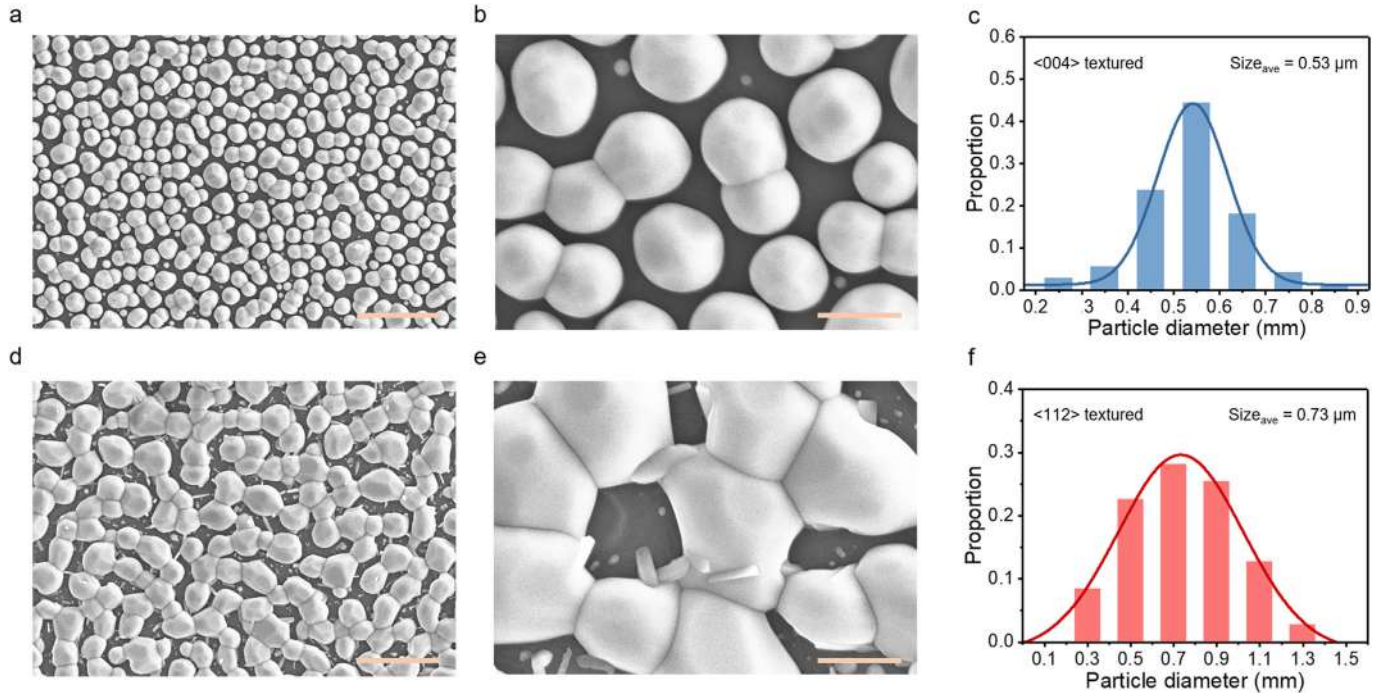

Fig. 3. SEM images and size distribution of < 004 > -textured (a, b and c) and < 112 > -textured (d, e and f) $BaMoO_4$: Eu^{3+} thin films. Scale bar: 5 μm.

$BaMoO_4$ thin films with different Eu^{3+} concentration are 663.9, 669.6, 664.9, 656.1, 645.2 μs, respectively. The decay time traces of $BaMoO_4$: Eu^{3+} thin films are illustrated in Fig. 5c, this reduction in average time (τ^*) is the result of the well-known concentration quenching. The distance among Eu^{3+} decreases with increasing doping concentration, resulting in increased nonradiative energy migration.

The Commission Internationale de l'Eclairage (CIE) chromaticity diagram of the optimal $BaMoO_4$: $0.05Eu^{3+}$ thin film is displayed in Fig. 6. The color coordinate of this sample is located at (0.6581, 0.3416) and marked as a green star.

The color purity (CP) can be calculated by the following equation [34]:

$$\text{color purity} = \frac{\sqrt{(x - x_i)^2 + (y - y_i)^2}}{\sqrt{(x_d - x_i)^2 + (y_d - y_i)^2}} \times 100\%$$

Where (x, y) presents the coordinate of the sample, (x_i, y_i) stands for the white illumination, (x_d, y_d) corresponds to the dominated wavelength of the sample. The coordinate of the sample is located at the edge of the CIE diagram, indicating that the color purity is close to 100%.

4. Conclusion

In summary, by engineering the grain orientation, we developed a cost-efficiency strategy to fabricate the $BaMoO_4$: Eu^{3+} thin films on the silicon substrates with controllable surface morphology and highly enhanced luminescence performances, by which the emission intensity of the < 004 > -textured thin film was enhanced to 366% compared to randomly oriented thin film equivalents. We systematically discussed the influence of the orientation of the substrate, annealing temperatures, layers of thin film, and concentrations of the doping ions on the shape, size, orientation, and photoluminescence performance of the $BaMoO_4$: Eu^{3+} thin films. With annealing temperature of 700 °C and doping concentration of 5%, the < 004 > -textured thin film demonstrated red emission at 615 nm with CCT of 2922 °C and ultra-high color purity of nearly 100%. The proposed tactic paves an alternative

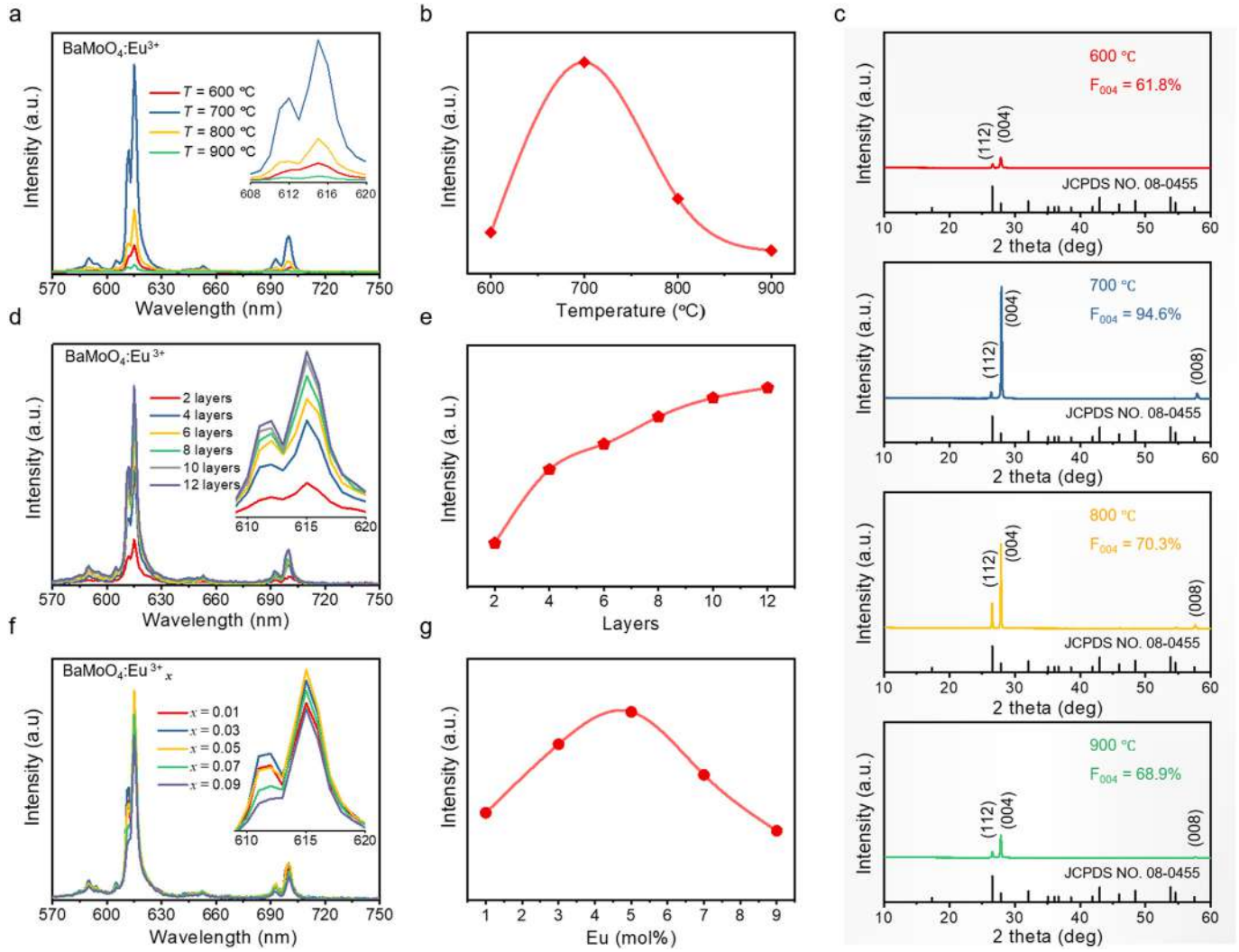

Fig. 4. The photoluminescence (PL) spectra and crystal structure of $BaMoO_4$: Eu^{3+} thin films mounted on (001)-oriented Si substrate. (a) The temperature-dependent emission spectra of $BaMoO_4$: Eu^{3+} thin films. (b) The emission intensity of $BaMoO_4$: Eu^{3+} thin films annealed at different temperatures. (c) The XRD pattern of $BaMoO_4$: Eu^{3+} thin films annealed at different temperatures (600, 700, 800 and 900 °C). (d) The layer-dependent emission spectra of $BaMoO_4$: Eu^{3+} thin films. (e) The emission intensity of $BaMoO_4$: Eu^{3+} thin films with various layers. (f) The emission spectra of $BaMoO_4$: Eu^{3+} thin films with various doping concentrations. (g) The emission intensity of $BaMoO_4$: Eu^{3+} thin films with various doping concentrations.

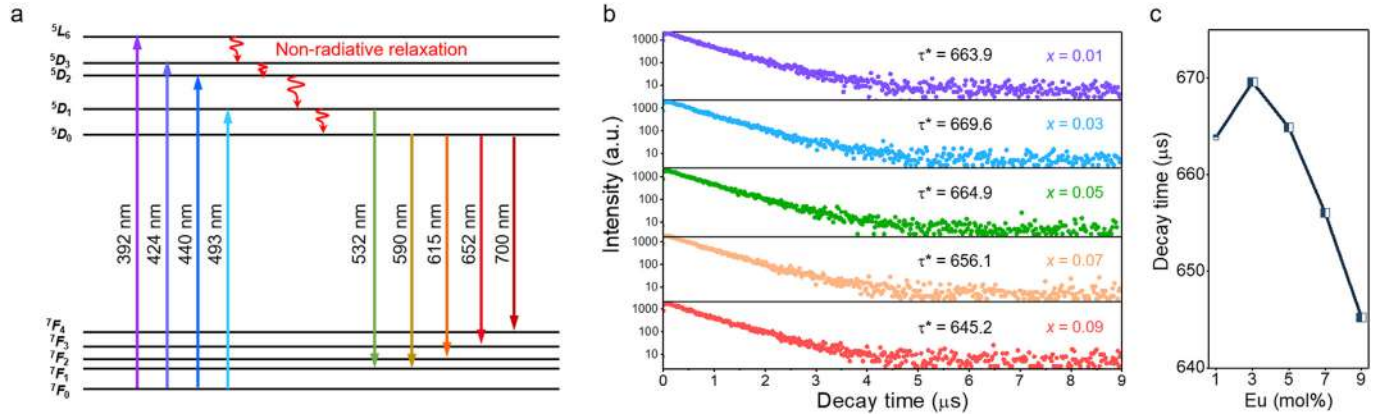

Fig. 5. (a) The diagram of the luminescence mechanism of Eu^{3+} ion-doped $BaMoO_4$ thin films. (b) PL decay curves of $BaMoO_4$: Eu^{3+} thin films with different doping concentration under an excitation wavelength of 300 nm. (c) The decay time traces of $BaMoO_4$: Eu^{3+} thin films.

Table 1
Summary of lifetime fitting parameters of the $BaMoO_4$: Eu_x^{3+} thin films.

x	τ_1 (μs)	f_1 (%)	τ_2 (μs)	f_1 (%)	τ_{avg} (μs)	x^2
0.01	468.74	29.31	744.82	70.69	663.90	2.33
0.03	491.23	40.25	789.75	59.75	669.60	2.05
0.05	580.93	77.88	960.55	22.12	664.90	2.00
0.07	517.44	47.21	780.03	52.79	656.06	2.02
0.09	329.79	14.30	697.85	85.70	645.23	2.34

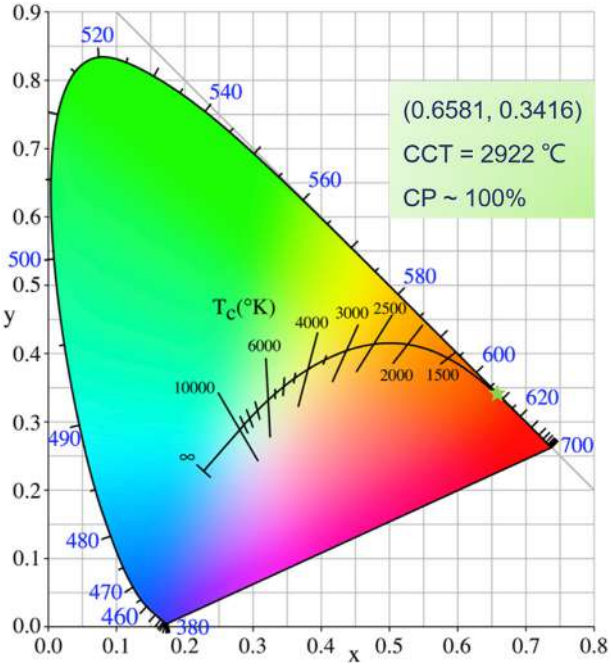

Fig. 6. CIE chromaticity diagram of Eu^{3+} ion-doped $BaMoO_4$ thin film (annealing temperature = 700 °C, layers = 10, and doping concentration = 0.05).

pathway for preparing high-efficiency luminescent thin films, and shows great potential in endowing luminescent thin film with a wide range of practical applications.

Declaration of competing interest

The authors declare that they have no known competing financial interests or personal relationships that could have appeared to influence the work reported in this paper.

Acknowledgments

This work is supported by the National Natural Science Foundation of China (No.61801403), Young Scientific and Technological Innovation Research Team Funds of Sichuan Province (No.20CXTD0106), the Fundamental Research Funds for the Central Universities of China (A0920502051619-72).

References

[1] Y. Zhang, J. Hao, Metal-ion doped luminescent thin films for optoelectronic applications, J. Mater. Chem. C 1 (36) (2013) 5607–5618.
[2] A. Yousif, R.M. Jafer, S. Som, M.M. Duvenhage, E. Coetsee, H.C. Swart, The effect of different annealing temperatures on the structure and luminescence properties of Y_2O_3: Bi^{3+} thin films fabricated by spin coating, Appl. Surf. Sci. 365 (2016) 93–98.
[3] A. Scarangella, F. Fabbri, R. Reitano, F. Rossi, F. Priolo, M. Miritello, Visible emission from bismuth-doped yttrium oxide thin films for lighting and display applications, Sci. Rep. 7 (2017) 17325.
[4] X. Chen, G. Xiang, F. Chai, Z. Zhang, S. Shi, F. Xu, J. Zhao, An alternate spin-coating strategy toward high-quality polycrystalline thin Lu_2O_3: Eu^{3+} film fabrication, Surf. Coating. Technol. 302 (2016) 523–527.
[5] J.S. Bae, S.B. Kim, J.H. Jeong, J.-C. Park, D.-K. Kim, S.-H. Byeon, S.-s. Yi, Photoluminescence characteristics of Li-doped Y_2O_3: Eu^{3+} thin film phosphors, Thin Solid Films 471 (2005) 224–229.
[6] W. Deng, F. Chun, W. Li, H. Su, B. Zhang, M. Xie, H. Zhang, X. Chu, L. Jin, C. Luo, W. Yang, Structural and optical investigations of quasi-single crystal Eu^{3+}-doped $BaWO_4$ thin films, Langmuir 34 (29) (2018) 8499–8507.
[7] S. Cho, Photoluminescent properties of Tb-doped $SrMoO_4$ thin films deposited on quartz substrates, Solid State Sci. 101 (2020) 106155.
[8] F. Chun, W. Li, B. Zhang, W. Deng, X. Chu, H. Su, H. Osman, H. Zhang, X. Zhao, W. Yang, Visible and near-infrared luminescent properties of Pr^{3+} doped strontium molybdate thin films by a facile polymer-assisted deposition process, J. Colloid Interface Sci. 531 (2018) 181–188.
[9] R. Krishnan, H.C. Swart, J. Thirumalai, P. Kumar, Depth profiling and photometric characteristics of Pr^{3+} doped $BaMoO_4$ thin phosphor films grown using (266 nm Nd-YAG laser) pulsed laser deposition, Appl. Surf. Sci. 488 (2019) 783–790.
[10] H. Yu, X. Shi, L. Huang, X. Kang, D. Pan, Solution-deposited and low temperature-annealed Eu^{3+}/Tb^{3+}-doped $CaMoO_4$/$SrMoO_4$ luminescent thin films, J. Lumin. 225 (2020) 117371.
[11] Z. Xia, D. Chen, Synthesis and luminescence properties of $BaMoO_4$: Sm^{3+} phosphors, J. Am. Ceram. Soc. 93 (5) (2010) 1397–1401.
[12] L.K. Bharat, S.H. Lee, J.S. Yu, Synthesis, structural and optical properties of $BaMoO_4$: Eu^{3+} shuttle like phosphors, Mater. Res. Bull. 53 (2014) 49–53.
[13] S. Li, L. Yu, J. Sun, X. Man, Synthesis and photoluminescent characteristics of Eu^{3+}-doped $MMoO_4$ (M = Sr, Ba) nanophosphors by a hydrothermal method, J. Rare Earths 35 (4) (2017) 347–3355.
[14] J. Lin, Z. Zeng, Q. Ma, Q. Wang, Y. Zhang, Effects of multiple irradiations on luminescent materials and energy savings – a case study for the synthesis of $BaMO_4$: Ln^{3+} (M = W, Mo; Ln = Eu, Tb) phosphors, Energy 64 (2014) 551–556.
[15] Y. Xia, X. Zou, H. Zhang, M. Zhao, X. Chen, W. Jia, C. Su, J. Shao, Luminescence and energy transfer studies of Eu^{3+}-Tb^{3+} co-doped transparent glass ceramics containing $BaMoO_4$ crystallites, J. Alloys Compd. 774 (2019) 540–546.
[16] B. Wu, W. Yang, H. Liu, L. Huang, B. Zhao, C. Wang, G. Xu, Y. Lin, Fluorescence spectra and crystal field analysis of $BaMoO_4$: Eu^{3+} phosphors for white light-emitting diodes, Spectrochim. Acta: Mol. Biomol. Spectrosc. 123 (2014) 12–17.
[17] S.D. Bu, M.K. Lee, C.B. Eom, W. Tian, X.Q. Pan, S.K. Streiffer, J.J. Krajewski, Perovskite phase stabilization in epitaxial $Pb(Mg_{1/3}Nb_{2/3})O_3$–$PbTiO_3$ films by deposition onto vicinal (001) $SrTiO_3$ substrates, Appl. Phys. Lett. 79 (21) (2001) 3482–3484.
[18] Z. Liu, Y. Li, Sol-gel synthesis and luminescence property of ZnO:(La, Eu)Cl nanocomposite thin films, Thin Solid Films 516 (16) (2008) 5557–5561.
[19] T. Ohnishi, M. Lippmaa, T. Yamamoto, S. Meguro, H. Koinuma, Improved stoichiometry and misfit control in perovskite thin film formation at a critical fluence by pulsed laser deposition, Appl. Phys. Lett. 87 (24) (2005).
[20] R. Ghosh, D. Basak, S. Fujihara, Effect of substrate-induced strain on the structural, electrical, and optical properties of polycrystalline ZnO thin films, J. Appl. Phys. 96 (5) (2004) 2689–2692.
[21] T.M. McCleskey, P. Shi, E. Bauer, M.J. Highland, J.A. Eastman, Z.X. Bi, P.H. Fuoss, P.M. Baldo, W. Ren, B.L. Scott, A.K. Burrell, Q.X. Jia, Nucleation and growth of epitaxial metal-oxide films based on polymer-assisted deposition, Chem. Soc. Rev. 43 (7) (2014) 2141–2146.
[22] G.F. Zou, J. Zhao, H.M. Luo, T.M. McCleskey, A.K. Burrell, Q.X. Jia, Polymer-assisted-deposition: a chemical solution route for a wide range of materials, Chem. Soc. Rev. 42 (2) (2013) 439–449.
[23] E.C. Xiao, J. Li, J. Wang, C. Xing, M. Guo, H. Qiao, Q. Wang, Z.M. Qi, G. Dou, F. Shi, Phonon characteristics and dielectric properties of $BaMoO_4$ ceramic, J. Materiomics 4 (4) (2018) 383–389.
[24] M. Bazarganipour, Synthesis and characterization of $BaMoO_4$ nanostructures prepared via a simple sonochemical method and their degradation ability of methylene blue, Ceram. Int. 42 (11) (2016) 12617–12622.
[25] F.K. Lotgering, Topotactical reactions with ferrimagnetic oxides having hexagonal crystal structures—I, J. Inorg. Nucl. Chem. 9 (2) (1959) 113–123.
[26] J. Li, Z. Shen, X. Chen, S. Yang, W. Zhou, M. Wang, L. Wang, Q. Kou, Y. Liu, Q. Li, Z. Xu, Y. Chang, S. Zhang, F. Li, Grain-orientation-engineered multilayer ceramic capacitors for energy storage applications, Nat. Mater. (2020), https://doi.org/10.1038/s41563-020-0704-x.
[27] M.C. Oliveira, L. Gracia, I.C. Nogueira, M.F.C. Gurgel, J.M.R. Mercury, E. Longo, J. Andrés, On the morphology of $BaMoO_4$ crystals: a theoretical and experimental approach, Cryst. Res. Technol. 51 (10) (2016) 634–644.
[28] F. Chun, B. Zhang, H. Su, H. Osman, W. Deng, W. Deng, H. Zhang, X. Zhao, W. Yang, Preparation and luminescent properties of self-organized broccoli-like $SrMoO_4$: Pr^{3+} superparticles, J. Lumin. 190 (2017) 69–75.
[29] J. Li, Q. Liang, Y. Cao, J. Yan, J. Zhou, Y. Xu, L. Dolgov, Y. Meng, J. Shi, M. Wu, Layered structure produced nonconcentration quenching in a novel Eu^{3+}-doped phosphor, ACS Appl. Mater. Interfaces 48 (2018) 41479–41486.
[30] M.A. Signore, A. Taurino, M. Catalano, M. Kim, Z. Che, F. Quaranta, P. Siciliano, Growth assessment of (002)-oriented AlN thin films on Ti bottom electrode deposited on silicon and kapton substrates, Mater. Des. 119 (2017) 151–158.
[31] Y. Tan, K. Liang, Z. Mei, P. Zhou, Y. Liu, Y. Qi, Z. Ma, T. Zhang, Strain induced magnetic anisotropy of high epitaxial Ni thin films grown on different oriented PMN-PT substrates, Ceram. Int. 44 (5) (2018) 5564–5568.
[32] F. Chun, B. Zhang, H. Liu, W. Deng, W. Li, M. Xie, C. Luo, W. Yang, Na^+ and Pr^{3+} co-doped orange-emitting $CaYAl_3O_7$ phosphors: synthesis, luminescence properties and theoretical calculations, Dalton Trans. 47 (48) (2018) 17515–17524.
[33] X. Zhang, J. Wang, L. Huang, F. Pan, Y. Chen, B. Lei, M. Peng, M. Wu, Tunable luminescent properties and concentration-dependent, site-preferable distribution of Eu^{2+} ions in silicate glass for white LEDs applications, ACS Appl. Mater. Interfaces 7 (18) (2015) 10044–10054.
[34] Q. Zhang, X. Wang, Y. Wang, A novel germanate based red-emitting phosphor with high efficiency, high color purity and thermal stability for white light-emitting diodes and field emission displays, Inorg. Chem. Front. 7 (4) (2020) 1034–1045.